

Pushover analysis of confined masonry walls using a 3D macro-modelling approach



Jhair Yacila^{a,*}, Guido Camata^b, Jhoselyn Salsavilca^a, Nicola Tarque^a

^a Pontificia Universidad Católica del Perú, Department of Civil Engineering, Lima, Peru

^b Università degli Studi Gabriele D'Annunzio, Department of Engineering and Geology, Pescara, Italy

ARTICLE INFO

Keywords:

Macro-modelling
Confined masonry
Pushover
Dynamic explicit analysis

ABSTRACT

This paper shows a novelty way to simulate the nonlinear behaviour of confined masonry walls subjected to in-plane lateral loading by using a 3D macro-modelling approach. For this purpose, the finite elements method implemented in ABAQUS software was used. All the 3D solid finite elements were modelled as a single part, which allowed avoiding modelling the contact interfaces between concrete and masonry elements. The nonlinear behaviour of the concrete and masonry were governed by two main types of failures: crushing and cracking, which were properly represented by the Concrete Damage Plasticity (CDP) model. Steel rebars were modelled as elastic-plastic with hardening and were assumed to have a perfect adhesion with the surrounding concrete by means of the embedded constraint. Prior to the modelling process, experiments were carried out whose results were used as patterns to validate the proposed model. A calibration process of the tensile properties of masonry was conducted for properly fitting the experimental patterns. As a result, there were good agreements between the numerical and experimental outcomes in terms of capacity curves and cracking patterns.

1. Introduction

Confined masonry buildings are the most common type of construction for dwellings in Peru and other South American countries. The major issue with many of these constructions is their informality: According to [1], masonry dwellings constitute 84% of the total buildings in Peru and 60% of them did not have any engineering participation. Additionally, just in Lima, 9 out of 10 masonry dwellings were built by using bricks with a percentage of voids between 40% and 50%, which mean bricks with a density lower than that required by the Peruvian seismic code [2]. Fig. 1 shows a common case of masonry dwellings in Lima of up to five stories.

Peruvian seismic events have revealed the poor quality of these informal masonry dwellings, which has been responsible for human and material losses. However, this is not only related to the informality of the masonry constructions, but also to the lack of knowledge of the nonlinear behaviour of the masonry. For this reason, much research around the world has been devoted to experimental studies of the nonlinear behaviour of masonry walls, either for in-plane or out-plane loads [4–7]. However, such studies need economic resources, which are often scarce. To overcome this issue, numerical modelling is an alternative way to study this topic, since it allows replacing economic resources by computational resources.

In literature, many alternatives can be found for assessing the seismic vulnerability of masonry constructions in terms of the seismic hazard and the seismic response of the masonry walls during an earthquake [8]. For instance, the simplified evaluation methods offer different levels of evaluation which are related to a more refined knowledge in terms of geometrical and constructions details, materials characterization, surveys, visual inspections, among others. These levels of evaluation range from a territorial scale evaluation up to the location of specific damaged parts in a construction [9]. On the other hand, the analytical methods offer a simple way of evaluating some seismic parameters such as the maximum lateral load capacity and lateral stiffness, both related to the response of the masonry walls during an earthquake. In this sense, many analytical expressions have been proposed by different authors after conducting a great quantity of tests. As a result, these expressions have been adopted by different design codes due to their ability to predict with a reasonable accuracy the seismic parameters aforementioned [10]. Other analytical tool, which can be found in the literature, is the well-known Strut and Tie Method (STM) where the masonry is treated as an equivalent strut. This method is a powerful tool since no sophisticated computations are needed to evaluate the lateral load capacity of the masonry walls [11]. Finally, the Finite Element Method (FEM) appears as a more accurate tool to evaluate completely the seismic response of masonry walls due

* Corresponding author.

E-mail address: jhair.yacila@pucp.edu.pe (J. Yacila).



Fig. 1. Masonry dwellings in Lima [3].

to its potential of incorporating the nonlinear properties of all the materials. Within this framework, the macro-modelling approach, which means assuming all the materials as homogeneous, appears as a good alternative in case of a high refinement level is not needed. On the contrary, the micro-modelling approach, which means that all the components are modelled separately, including contact interfaces, appears as a good alternative in case of a high refinement level is needed. A third approach, known as simplified micro-modelling, results of combining the first two approaches and appears as a good alternative in case of an intermediate refinement level is needed [12].

Different numerical studies have been conducted to assess the behaviour of masonry walls subjected to in-plane lateral loads [13]. For instance, [14–16] used the macro-modelling technique to perform pushover analyses of confined masonry walls with different arrangements. In this case, the contact surface between the masonry and the concrete was considered as *Hard-Contact* for the normal direction and *frictional* for the shear direction. [11] On the other hand, [15,17] used the micro-modelling approach for masonry walls without confinement, for which the bricks, mortar and contact surfaces were modelled separately by taking into account their nonlinear behaviour. The nonlinear behaviour of the bricks and mortar were modelled by the well-known Concrete Damage Plasticity (CDP), whereas the contact between the blocks was modelled by cohesive elements with a thickness of 0 mm. Basically, the behaviour of the cohesive elements is governed by a linear-elastic behaviour until its maximum tensile or shear strength is reached. Subsequently, its nonlinear behaviour is governed by a softening part characterized by progressive damage. Once the maximum damage is reached, the cohesive elements are deleted and contact properties begin to be dominant. For this purpose, *hard-contact* and *frictional* properties were defined to be the normal and shear contact properties, respectively. Finally, [18–20] used the simplified micro-modelling approach for modelling the in-plane behaviour of in-fill masonry walls, and diagonal compression tests, respectively. Like micro-modelling, cohesive elements were used for contact between blocks, and a frictional behaviour was defined to be activated once cohesive elements exhausted their strength.

As the different studies have demonstrated, the nonlinear behaviour of the masonry walls is of great interest mainly where they are part of the building's structural system. In the present paper, an easy way of assessing structural parameters of masonry walls is presented by using the macro-modelling approach. For this purpose, full-scale confined masonry walls were modeled to be subjected under monotonic lateral displacements. Finally, the proposed model was carefully calibrated by comparing capacity curves and cracking patterns with those recorded in a experimental campaign conducted by Manchego and Pari [21].

2. Previous work

The previous work was carried out by Manchego and Pari [21], with collaboration of the current research group, and consisted in testing 6 full-scale confined masonry walls subjected to in-plane lateral cyclic loading at the Pontifical Catholic University of Peru. Three of these walls were subjected to a vertical load of 170 kN, which was intended to represent the weight of a three-floor building over a wall located on

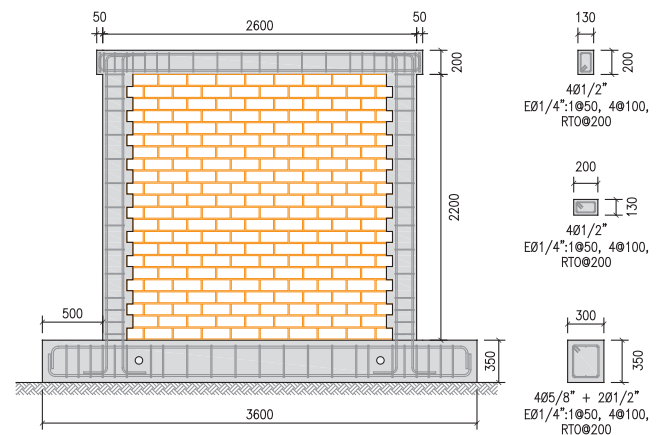


Fig. 2. Geometry and details of reinforcement of the walls tested in the previous work [21].

the first floor. This vertical load was applied prior to the application of lateral loads. The other three walls were only subjected to lateral cyclic loads. In addition, all of these walls were built by common workmanship in order to get the usual features of confined masonry walls in Peruvian dwellings.

2.1. Geometry and steel reinforcement of the tested walls

Fig. 2 shows the typical assemblage of the tested walls. Note the toothed connection between the confining columns and the masonry panel. Different studies, such as the one conducted by Singhal and Durgesh [10], have demonstrated the effectiveness of this type of connection to significantly improve the post-peak behaviour of confined masonry walls when are subjected to in-plane lateral loads. Regarding to the confining elements, since the main aim of them is to avoid the quick disintegration of the masonry panel, as well as providing more ductility, typical practice is to provide corrugated steel reinforcement with a diameter of $\phi 1/2''$ as longitudinal reinforcement and $\phi 1/4''$ as transverse stirrups. It should be mentioned that in a real confined masonry dwelling, beam foundations of reinforced concrete are not built. In contrast, beams of cyclopean concrete are employed. Nevertheless, due to the need of hoisting and fixing the walls prior testing, reinforced concrete was essential. On the other hand, the foundation is often assumed as rigid enough, so that it can also be modeled as a fixed boundary condition without influencing the nonlinear response of the confined masonry walls.

2.2. Testing setup

Fig. 3 shows the typical assemblage that was used to carry out the cyclic tests. The lateral displacements were imposed by means of a dynamic actuator, which was controlled by displacements on a computer. This actuator was intended to be fixed to a reaction frame rigid enough to avoid distorted lateral displacements. On the other hand, one hydraulic jack was located at each end of the foundation to prevent it from being overturned. In addition, one hydraulic jack was located at one of the ends of the foundation to prevent its sliding horizontally in one direction. In the other direction, the foundation was intended to react against the rigid reaction frame. The vertical load, where it was applied, was imposed by an additional hydraulic jack, which in turn was connected to two rigid steel beams, in order to distribute as much as possible the vertical load over the wall's confining beam.

2.3. Experimental results

In order to compare the pushover analysis conducted in this paper with the cyclic experimental test conducted by [21], only the envelope

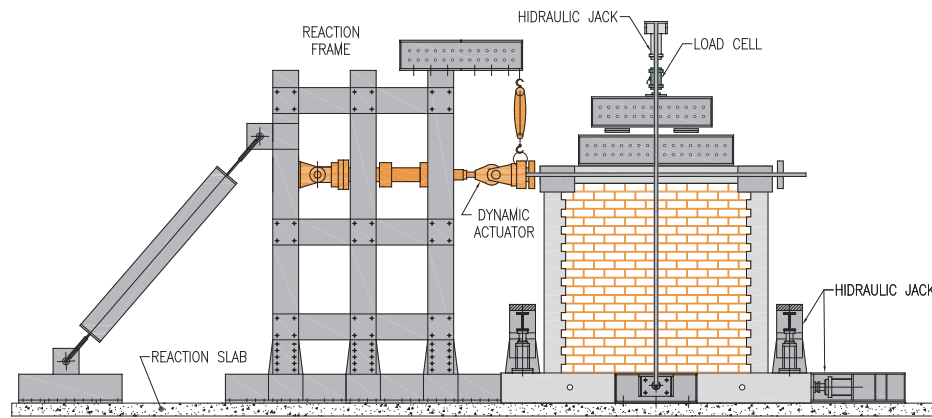
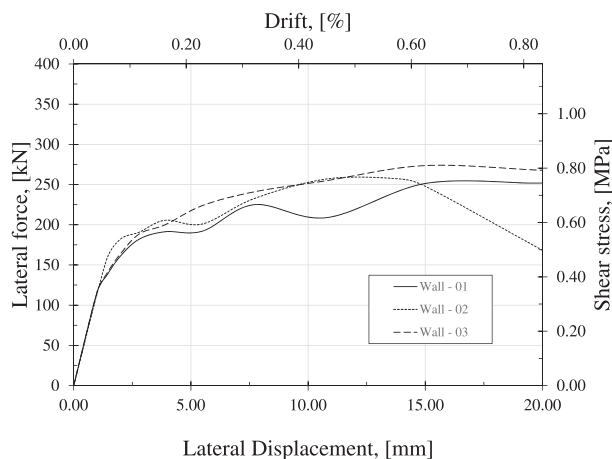
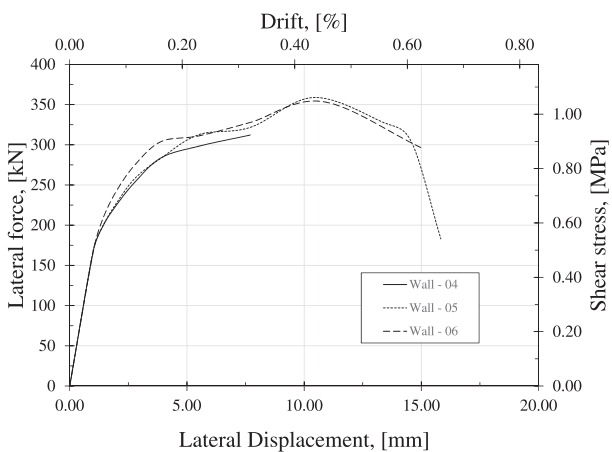


Fig. 3. Testing setup of the walls tested in the previous work [21].



(a) without vertical load



(b) with vertical load

Fig. 4. Experimental envelope curves of the walls.

curve in the pushing direction was taken into account. Fig. 4 shows these envelope curves for both walls with and without vertical load. Note that the shear stresses shown on the secondary vertical axis do not correspond to the real stresses, but to nominal stresses computed as the ratio between the lateral forces and the cross-sectional area of the walls.

Experimental tests on small samples were also carried out in order to characterize the material properties involved in the confined masonry walls with and without vertical load. For instance, uniaxial compressive tests of brick prisms were conducted to get the

compressive strength and Young’s modulus of the masonry. In addition, uniaxial diagonal compressive tests were conducted over small square masonry walls in order to get their tensile strength. Typical compressive tests of cylindrical specimens were carried out for each concrete element (foundation, column and beam), in order to get their compressive strength. It should be noted that every small sample was taken from each kind of tested wall (with and without vertical load) by considering they were built on different dates. The experimental results of these tests are shown in Table 1.

3. Finite element model

In this research, the macro-modelling approach has been adopted. In this way, the bricks, mortar, concrete, and their contact interfaces were not modelled separately. Rather, all components were treated as homogeneous and isotropic materials. The modelling process was carried out in the commercial software package ABAQUS. The foundation and wall were intended to be a single part, which meant that each contact between different materials was assumed to be monolithic. This assumption was made because of the constructive typology of the confined masonry. Namely, in this kind of constructions, the masonry panel is built prior to the casting of the confining elements. This fact added to the toothed connection often used between masonry and columns make all the components work as monolithic.

Except for the steel reinforcement, all the components were modelled as continuum three-dimensional elements with 8 nodes with reduced integration (C3D8R). The steel rebars were modelled as truss three-dimensional elements with two nodes (T3D2). The interaction between the steel rebars and the surrounding concrete was considered as perfect adhesion, implemented by means of an embedded constraint. This means that no slip was taken into account between these two

Table 1
Mechanical properties of materials.

Material	E_0 [MPa]	ν [-]	f'_{cm} [MPa]	$f_{lm}(f_y)$ [MPa]	G_{ch} [N/mm]	G_f [N/mm]
<i>Wall without vertical load</i>						
Foundation’s concrete	25,900	0.15	27.50	2.75	13.70	0.137
Column’s concrete	21,300	0.15	16.50	1.95	8.60	0.120
Beam’s concrete	27,500	0.15	31.50	3.00	14.90	0.136
Masonry	5700	0.15	10.00	1.40	-	0.12
Steel rebars	200,000	0.30	-	(420)	-	-
<i>Wall with vertical load</i>						
Foundation’s concrete	25,900	0.15	27.50	2.75	13.70	0.137
Column’s concrete	24,400	0.15	23.50	2.47	11.60	0.129
Beam’s concrete	27,100	0.15	30.50	2.94	14.50	0.135
Masonry	5700	0.15	10.00	1.40	-	0.12
Steel rebars	200,000	0.30	-	(420)	-	-

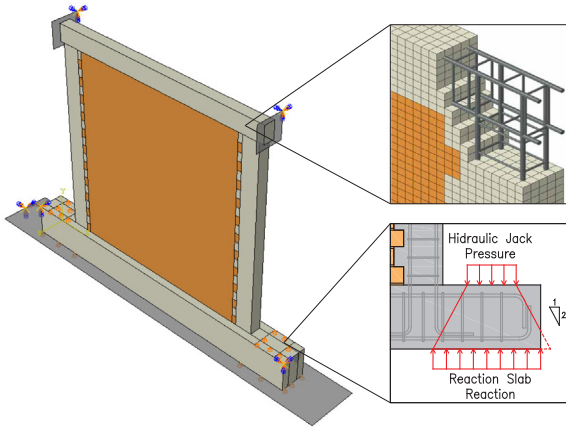


Fig. 5. Schematic of the numerical model.

materials.

As boundary conditions, each wall was assumed to be over an analytical rigid surface which represents the reaction slab shown in Fig. 3. The hydraulic jack and reaction frame intended to prevent the horizontal sliding of the foundation, as well as the dynamic actuator, were also modelled as analytical rigid surfaces. The hydraulic jacks which were intended to prevent the foundation from overturning were modelled as pin supports where only the vertical component was restricted. However, these hydraulic jacks had an unknown initial pressure prior to the cyclic testing, which in turn was increasing while the lateral displacements were increasing. This fact was intended to be modelled by assuming that a certain area below the foundation did not suffer vertical displacements like its corresponding restricted top area. For this purpose, it was assumed that the transmission of pressure between these hydraulic jacks and the reaction slab had a slope of 1:2, as shown in Fig. 5.

A variant of classical plasticity theory with the introduction of damage concepts is commonly used with *Concrete Damage Plasticity* to simulate the nonlinear behaviour of quasi-brittle materials. However, its accuracy is questionable, due to its tensile behaviour formulation [22]. Even when the tensile stiffness degradation is properly simulated, as is shown by some experimental tensile cyclic tests [23], this may fail when strong excursions between the tensile and compressive strains take place. Since the main objective of the present work is to get the capacity curve of the walls, pushover analyses were carried out. In this way, severe changes between the tensile and compressive strains were intended to be avoided.

3.1. Concrete Damage Plasticity

Concrete Damage Plasticity (CDP) is a continuum plasticity-based damage model for concrete and other quasi-brittle materials in any type of structure. It is assumed that the failure of a material is governed by two main mechanisms: tensile cracking and compressive crushing. The evolution of its yield surface, which is defined by Eq. (1), is controlled by two hardening variables, $\tilde{\epsilon}_t^{pl}$ and $\tilde{\epsilon}_c^{pl}$, which are the tensile and compressive equivalent plastic strain, respectively.

$$F = \frac{1}{1-\alpha}(\bar{q} - 3\alpha\bar{p} + \beta(\tilde{\epsilon}^{pl})(\hat{\sigma}_{max}) - \gamma(-\hat{\sigma}_{max})) - \bar{\sigma}_c(\tilde{\epsilon}_c^{pl}) \leq 0 \quad (1)$$

where \bar{p} is the effective hydrostatic pressure, \bar{q} is the von Mises equivalent effective stress, $\hat{\sigma}_{max}$ is the maximum eigenvalue of $\hat{\sigma}$, and $\beta(\tilde{\epsilon}^{pl})$ is the function defined by

$$\beta(\tilde{\epsilon}^{pl}) = \frac{\bar{\sigma}_c(\tilde{\epsilon}_c^{pl})}{\bar{\sigma}_t(\tilde{\epsilon}_t^{pl})}(1-\alpha) - (1+\alpha) \quad (2)$$

where $\bar{\sigma}_t$ and $\bar{\sigma}_c$ are the tensile and compression effective stress, respectively. The parameter α can be obtained experimentally with the

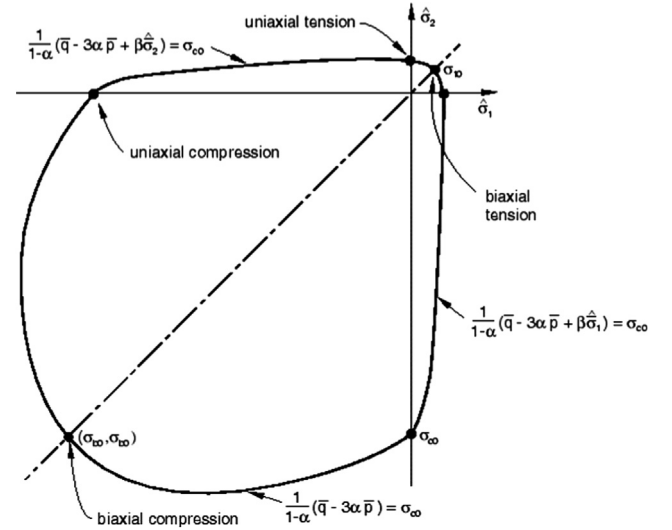


Fig. 6. Yield surface of CDP for plane stress conditions [25].

following expression:

$$\alpha = \frac{\sigma_{b0} - \sigma_{c0}}{2\sigma_{b0} - \sigma_{c0}} \quad (3)$$

where σ_{b0} and σ_{c0} are the failure stress for biaxial and uniaxial conditions, respectively. The parameter γ is defined as

$$\gamma = \frac{3(1 - K_c)}{2K_c - 1} \quad (4)$$

where K_c is a constant that can be obtained experimentally through triaxial tests [24]. Finally, CDP uses a potential flow, G , which is governed by the Drucker–Prager hyperbolic function

$$G = \sqrt{(e\sigma_{t0}\tan\psi)^2 + \bar{q}^2} - \bar{p}\tan\psi \quad (5)$$

where ψ is the dilation angle measured in the $p - q$ plane with a high level of confinement pressure, σ_{t0} is the uniaxial tensile strength, and e is an eccentricity that defines the rate at which the function reaches the asymptote. A typical yield surface for plane stress conditions is shown in Fig. 5. The intersection between the yield boundary and principal axes represents both the compressive and tensile uniaxial strength of the material. As is characteristic of quasi-brittle materials, a reduced biaxial tension and increased biaxial compression are also illustrated in Fig. 6 [18].

All the parameters involved in CDP can be obtained from uniaxial, biaxial and triaxial tests, as described by Jankowiak and Lodygowski [24]. Regarding the dilation angle, ψ , values of 30° and 35° were used for concrete and masonry, respectively, as were correctly used by [7]. Regarding the rest of parameters, in the absence of experimental data, e , σ_{b0}/σ_{c0} and K_c were taken with their default values from ABAQUS to be: 0.1, 1.16 and 0.667, respectively [25]. Regarding the parameter of viscosity, it was taken to be 0.0001, following the recommendations of [26]. For a better understanding of the CDP model, revise [25].

3.2. Material models

According to the configuration of the tested walls, 5 different materials were considered for modelling: (1) the foundation's concrete, (2) the column's concrete, (3) the beam's concrete, (4) the masonry, and (5) the rebar's steel. Table 1 shows their mechanical properties, which were used for modelling purposes, where E is the Young's modulus, ν is the Poisson's ratio, f'_c is the compressive strength, f'_t is the tensile strength, f_y is the yield strength, G_{ch} is the crushing energy, and G_f is the fracture energy of the materials.

Regarding the constitutive laws of concrete and masonry, it is

known that their behaviour lies between ideal brittle and ductile. In fact, they are closer to a brittle behaviour than ductile, therefore, both are considered as quasi-brittle materials [27]. In the following subsections, the constitutive models adopted for the concrete, masonry and steel reinforcement will be discussed.

3.2.1. Concrete

The compressive behaviour of concrete was represented by three main parts: (1) linear, (2) hardening and (3) softening. The linear part was taken to last up to a compressive stress equivalent of $0.4f'_{cm}$. The second part was characterized by a parabolic hardening, in compliance with CEB-FIP [28], up to the peak strength f'_{cm} and its associated strain ϵ_{cm} . The last part was taken as a hyperbolic softening, according to the recommendations of Krätzig and Pölling [29]. Eq. (6) represents this formulation.

$$\sigma_{c(1)} = E_0 \epsilon_c \quad (6a)$$

$$\sigma_{c(2)} = \frac{E_{ci} \frac{\epsilon_c}{f_{cm}} - \left(\frac{\epsilon_c}{\epsilon_{cm}} \right)^2}{1 + \left(E_{ci} \frac{\epsilon_{cm}}{f_{cm}} - 2 \right) \frac{\epsilon_c}{\epsilon_{cm}}} f_{cm} \quad (6b)$$

$$\sigma_{c(3)} = \left(\frac{2 + \gamma_c f_{cm} \epsilon_{cm}}{2f_{cm}} - \gamma_c \epsilon_c + \frac{\epsilon_c^2 \gamma_c}{2\epsilon_{cm}} \right)^{-1} \quad (6c)$$

where

$$\gamma_c = \frac{\pi^2 f_{cm} \epsilon_{cm}}{2 \left[\frac{G_{ch}}{l_{eq}} - 0.5 f_{cm} \left(\epsilon_{cm} (1 - b) + b \frac{f_{cm}}{E_0} \right) \right]^2}$$

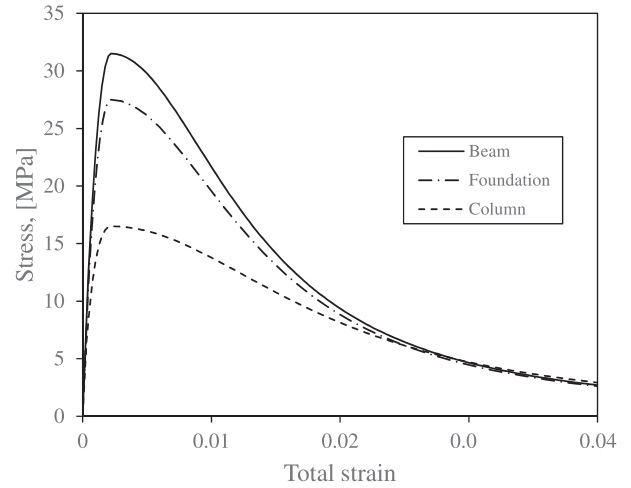
According to CEB-FIP [28], these parameters can be expressed as $\epsilon_{cm} = 0.0022$, $f_{cm} = f_{ck} + 8$, where f_{ck} is the characteristic compression strength. $E_{ci} = 10000 f_{cm}^{1/3}$ and $E_0 = (0.8 + 0.2 f_{cm} / 88) E_{ci}$, where E_0 is the modulus of the secant corresponding to a stress of $0.4 f_{cm}$. The stresses and modules of elasticity are expressed in [MPa]. G_{ch} is the crushing energy per unit area [Nmm/mm²]. l_{eq} is the characteristic length, which depends on the mesh size, type of element, and cracking direction [30]. In this paper, l_{eq} is taken equal to the chosen mesh size. This is so as to take into account the direction of the expected cracks on the concrete. Finally, b results from averaging the ratio $\epsilon_c^{pl} / \epsilon_c^{ch}$ over the relevant strain range. In this work, $b = 0.70$ was initially assumed, however, this value was later iterated until convergence was reached. Fig. 7 shows the stress–strain curves considered for concrete in compression.

Regarding the tensile behaviour, it was assumed to be governed by a first linear elastic part up to its tensile strength, at which point tensile failure begins. Thereafter, a post-failure behaviour of cracked concrete was intended to be defined in strain-softening terms. For this purpose, the formulation given by Hordijk [31] was selected. It is given by

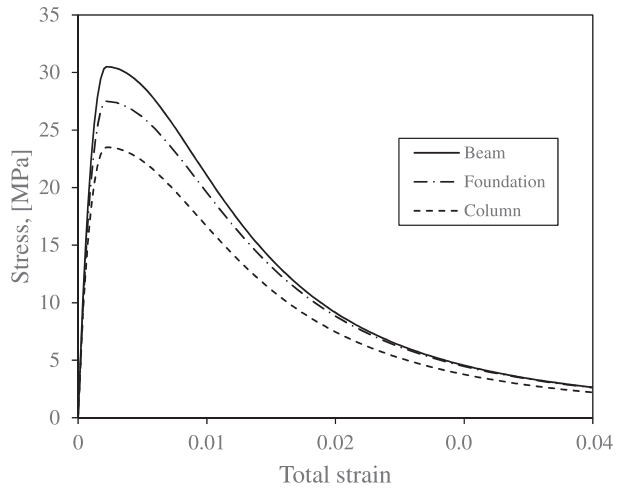
$$\sigma_{t(1)} = E_0 \epsilon_t \quad (7a)$$

$$\frac{\sigma_{t(2)}}{f_{tm}} = \left[1 + \left(c_1 \frac{w}{w_c} \right)^3 \right] e^{-c_2 \frac{w}{w_c}} - \frac{w}{w_c} (1 + c_1^3) e^{-c_2} \quad (7b)$$

where $c_1 = 3$, $c_2 = 6.93$ [31], w_c is a critical crack opening, for which $\sigma_{t(2)}$ becomes zero, which can be calculated as $w_c = 5.14 G_f / f_{tm}$. In addition, in the absence of experimental data, G_f may be estimated as $G_f = 0.073 f_{cm}^{0.18}$ [28]. Likewise, G_{ch} may be estimated as $G_{ch} = (f_{cm} / f_{tm})^2 G_f$ [32]. It should be noted that Eq. (7b) defines the post-failure tensile behaviour in terms of the crack opening w [mm]. However, in the case of reinforced concrete, the post-failure relation is usually expressed in terms of strains. In this way, it is intended to avoid any dependence of the results on the mesh size. For this purpose, the cracking strain was expressed as $\epsilon_{ck} = w / l_{eq}$. Fig. 8 shows the adopted post-failure stress–strain curves for the tensile behaviour of the concrete. It should be noted that a residual stress $\sigma_r = f_{tm} / 50$ was used to avoid kinetic instabilities.



(a) without vertical load



(b) with vertical load

Fig. 7. Stress–strain relations for concrete in compression.

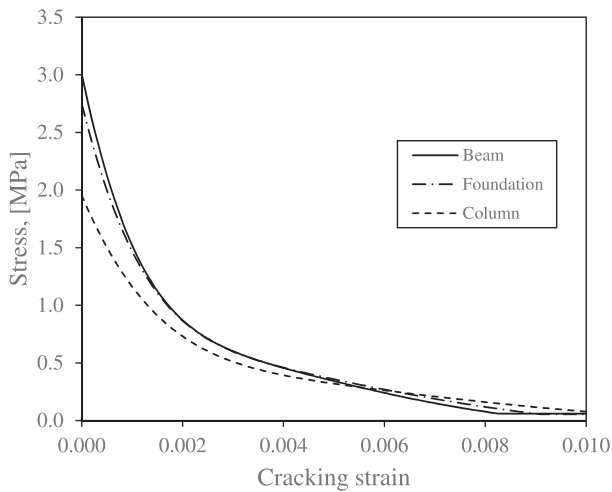
3.2.2. Masonry

The compressive behaviour of the masonry was represented by three main parts: (1) parabolic hardening, (2) linear softening and (3) residual, according to the constitutive model proposed by [33], as is shown in Fig. 9. It is worth highlighting that, a residual stress of $0.1 f_{cm}$, unlike Fig. 9, was taken into account to avoid kinetic instabilities [12].

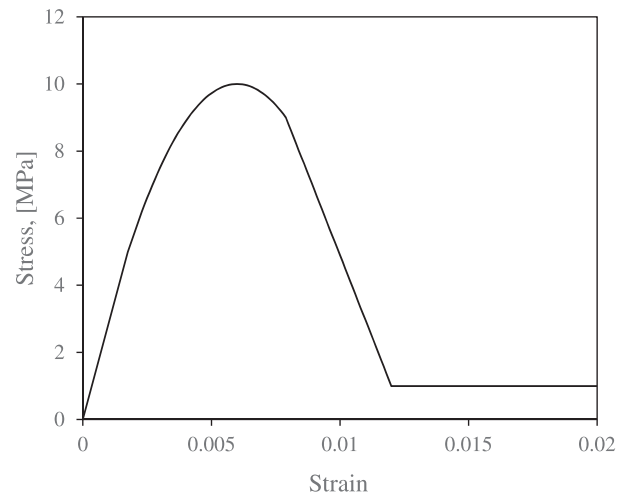
As with the concrete, the tensile behaviour was assumed to be governed at first by a linear-elastic part followed by nonlinear behaviour. In this case, a post-failure exponential softening was assumed [12]. However, it is worth noting that, unlike the reinforced concrete, the masonry panel does not have reinforcement, which would introduce an unreasonable mesh sensitivity into the results when a post-failure stress–strain curve is defined [25]. To address this problem, Hillerborg's fracture energy proposal was employed to define a post-failure stress–displacement curve (Eq. (8)) [35]. Fig. 10 shows the adopted curves for the masonry.

$$\sigma_{t(1)} = E_0 \epsilon_t \quad (8a)$$

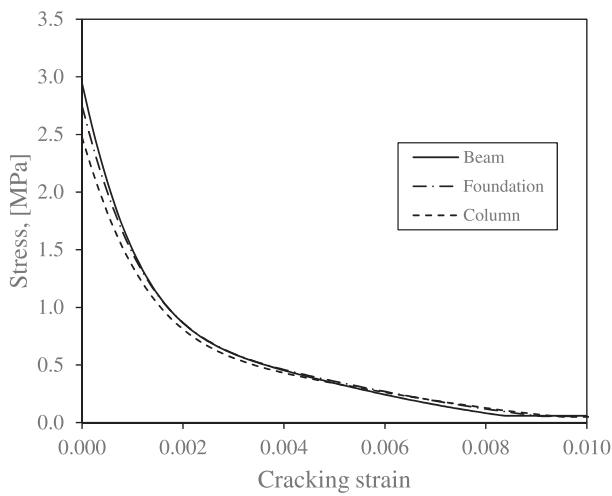
$$\sigma_{t(2)} = f_{tm} \exp \left(- \frac{f_{tm} w}{G_f} \right) \quad (8b)$$



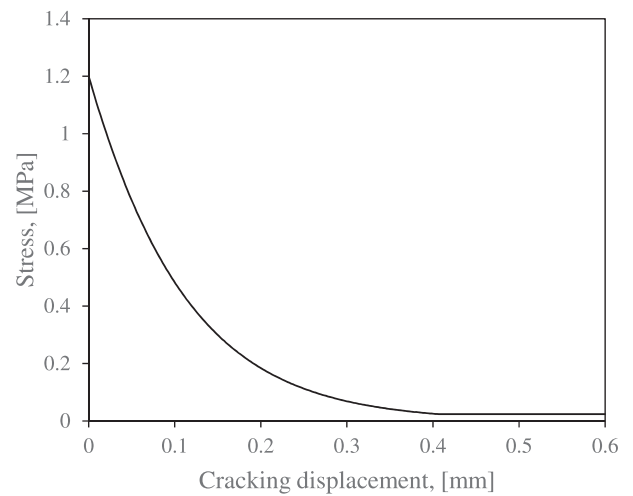
(a) without vertical load



(a) Compression



(b) with vertical load



(b) Traction

Fig. 8. Stress–strain relations for concrete in traction.

Fig. 10. Constitutive laws for masonry.

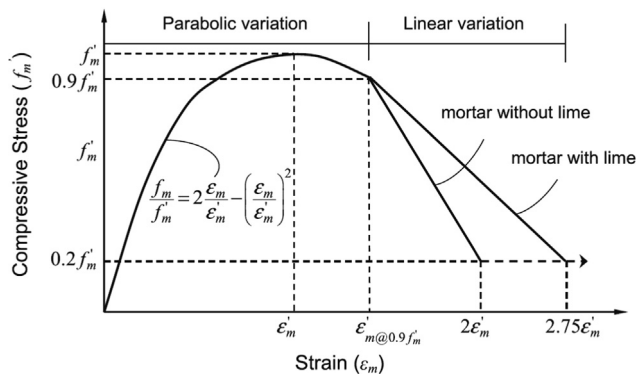


Fig. 9. Stress–strain formulation for masonry in compression [34].

3.2.3. Steel reinforcement

In cases where the behaviour of the reinforced concrete is what dominates, it is important to consider the *bond slip* effect between the steel reinforcement and the concrete. This effect is related to the fact that given a particular deformation of an RC element, the steel

reinforcement and the concrete have different strains due to the difference in their material properties (e.g. the Young and Poisson modules). This effect can be taken into account by modifying the constitutive law of the steel reinforcement [36]. Nevertheless, in the case of confined masonry walls, where the behaviour of the masonry is what dominates, no considerable differences result from considering the *bond slip* effect. For this reason, this paper does not take this effect into consideration. Anyway, in case the *bond slip* effects are needed to be considered for other considerations, the following literature could also be helpful [37–40].

On the other hand, the steel reinforcement was modelled as elastic–plastic with a hardening of 2%E slope between the strains related to the yield and ultimate stresses, ϵ_y and ϵ_u , respectively. The proposed constitutive law that takes into account the effect of bond-slip [36], considers a reduction of real yielding stress and young modulus of the steel bar. In this line, a resultant hardening slope of 3%E is derived from joining the points related to the fictitious elastic limit state and the ultimate limit state. In this case, such as no mechanical properties were modified, the considered hardening slope turned out from joining the points related to the well-known elastic limit state (ϵ_y, F_y), and the ultimate limit state (ϵ_u, F_u). Fig. 11 compares a typical experimental curve

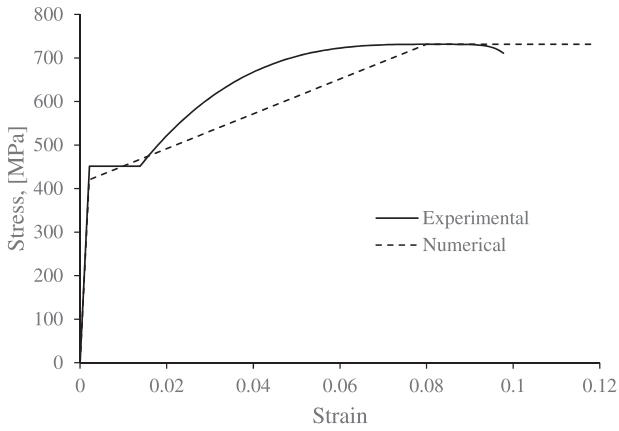


Fig. 11. Stress-strain curve for the steel reinforcement.

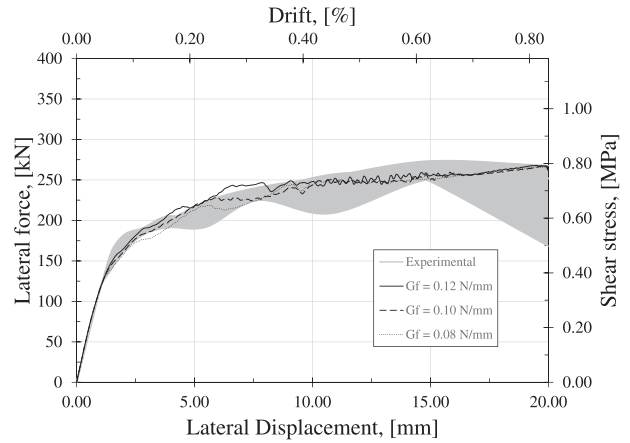


Fig. 14. Numerical responses to changes in the fracture energy of masonry ($E^* = 3705$ MPa, $t_f = 1.20$ MPa).

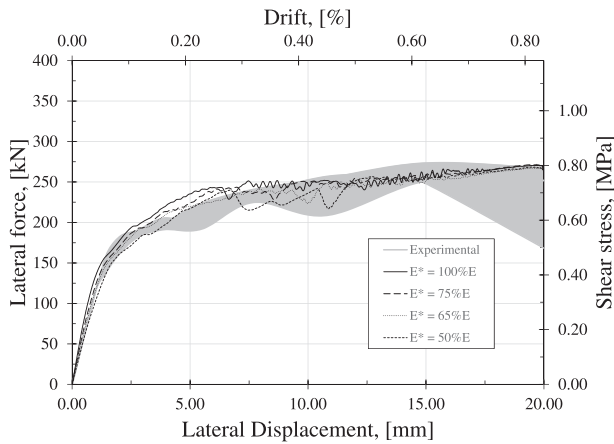


Fig. 12. Numerical responses to changes in the Young's modulus of masonry ($G_f = 0.12$ N/mm², $t_f = 1.40$ MPa).

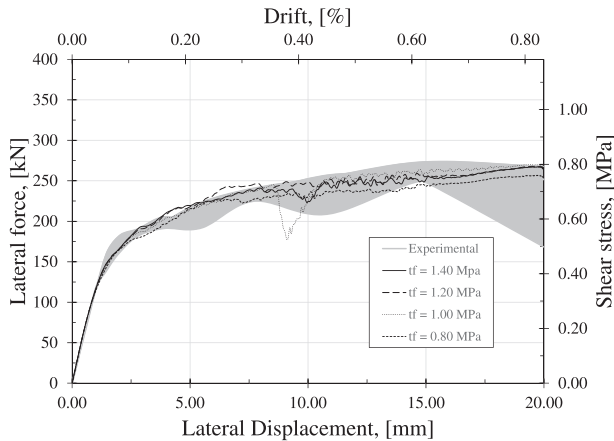


Fig. 13. Numerical responses to changes in the tensile strength of masonry ($E^* = 3705$ MPa, $G_f = 0.12$ N/mm).

for the steel reinforcement and the numerical curve adopted as the constitutive law.

3.3. Damage models

The damage parameters for both the compressive and tensile behaviour of the concrete were computed by following the formulation proposed by Alfarah et al. [30], which is an update of the formulation of Lee and Fenves [23]. On the other hand, the pivot rule formulation

proposed by Park et al. [41] was used for both the compressive and the tensile behaviour of the masonry.

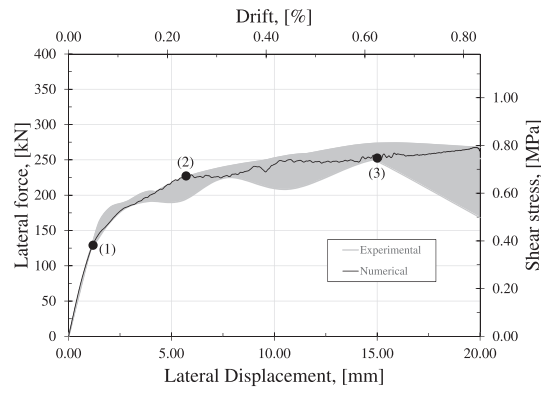
It is worth mentioning that even when a unit value of a damage parameter means a total failure of the material, which in turn means that the material can not carry more stress, this could not be applied to the model. This is related to the formulation of CDP [25], which states that a unit value of damage parameter would lead to an infinite value of the plastic strain. For this reason, in the present paper, all the damage parameters were fixed to have a maximum value of 0.98.

3.4. Quasi-static modelling

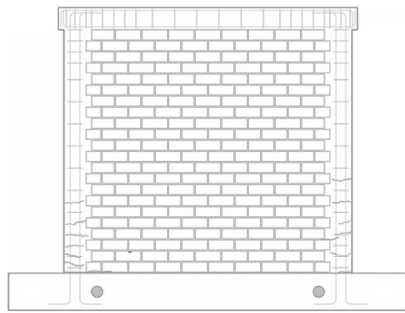
Experimentally, the cyclic tests of the walls were carried out slowly, as a quasi-static event, in order to avoid kinematic effects. For modelling quasi-static phenomena, ABAQUS offers two powerful solvers: implicit and explicit. The implicit solver involves the solution of static equilibrium equations by enforcing an equilibrium between the internal and external forces. If the implicit solver does not find a convergence between these forces in a specific time increment, it adds certain corrections through the Newton-Raphson method. The process continues until the difference between the internal and external forces is less than a small value, called the convergence criterion. However, to solve the equilibrium equations, the implicit solver needs to invert the stiffness matrix, which involves a high computational cost, depending on the number of degrees of freedom.

On the other hand, the explicit solver involves the solution of dynamic equilibrium equations. Unlike the implicit solver, the explicit solver does not enforce an equilibrium between the internal and external forces, which means that there is no convergence criterion. Moreover, the explicit solver needs to invert the mass matrix instead of the stiffness matrix, which turns out to be much cheaper computationally. Indeed, inverting an uncoupled diagonal mass matrix is less expensive than inverting a fully coupled stiffness matrix. Once the mass matrix has been inverted, the acceleration in a specific time increment is calculated. Thereupon, the velocity and displacements are calculated by means of the central difference method.

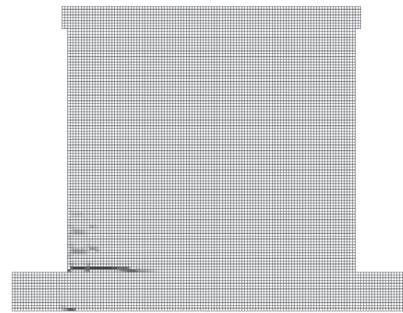
In general terms, an explicit solution moves away from the real solution if each time step is divided into only a few time increments. That is why the ABAQUS Explicit Solver efficiently implements a large number of time increments in order to obtain reliable results [25]. In this work, the explicit solver was used to model the quasi-static phenomena involved in the pushover analysis. Nevertheless, to avoid considerable kinematic effects, the kinetic energy was intended to kept less than 1% of the internal energy during the largest part of the test [42–44].



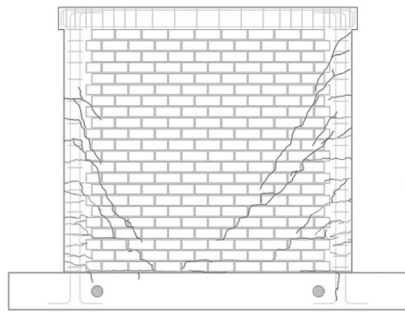
(a) Final numerical curve



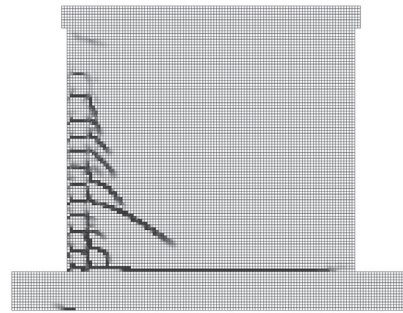
(b) (1) Experimental cyclic test



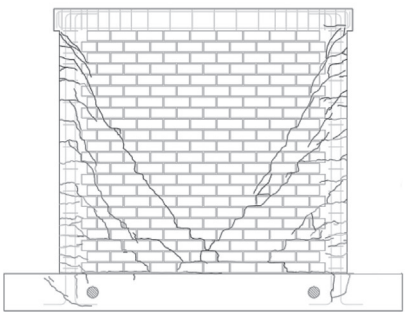
(c) (1) Numerical pushover



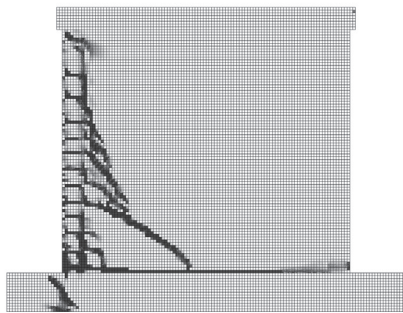
(d) (2) Experimental cyclic test



(e) (2) Numerical pushover



(f) (3) Experimental cyclic test



(g) (3) Numerical pushover

Fig. 15. Experimental and numerical cracking patterns for walls without vertical load ($E^* = 3705$ MPa, $t_f = 1.20$ MPa, $G_f = 0.10$ N/mm).

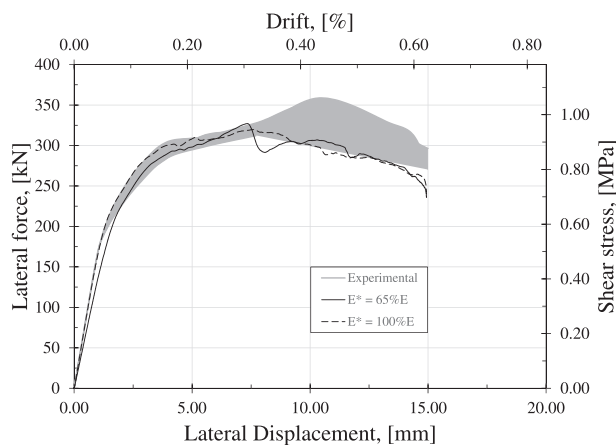


Fig. 16. Young's modulus calibration for the effect of the vertical load ($t_f = 1.20$ MPa, $G_f = 0.10$ N/mm).

4. Validation of the proposed model

4.1. Walls without vertical load

Taking into account that each wall was assumed to be a single part, a single mesh size would affect the entire part. Therefore, in order to find an appropriate mesh size, one that would require less computational cost without losing accuracy, a sensitivity analysis was carried out.

The Young's modulus of the masonry shown in Table 1 was computed experimentally by uniaxial compressive tests conducted perpendicularly to the bed joints. However, this value can not be used directly for modelling since it would lead to stiffer responses, as has also been observed by others [45]. This is related to the fact that the macro-modelling approach tries to simulate even totally anisotropic materials as isotropic. As with Young's modulus, all the material properties obtained experimentally from small specimen tests were expected to be calibrated for the macro-modelling. For this reason, many iterations were carried out by varying the material properties of the masonry and the concrete. For instance, the compressive strength of the column's concrete was varied and its influence was analyzed in terms of cracking pattern and capacity curve of the overall response of the wall and so on. As a result, it was noted that the properties related to the tensile behaviour of the masonry controlled the overall response of the confined masonry wall. Therefore, a subsequent parametric study was conducted by varying three main parameters of masonry: Young's modulus, tensile strength, and fracture energy. This had the aim of getting average values that would allow properly fitting the experimental curves and the visual cracking patterns. The parametric study began considering the material properties shown in Table 1.

Fig. 12 shows the numerical curves obtained from iterating the Young's modulus, where it is possible to note that an equivalent Young's modulus $E^* = 65\%E_0$ allowed to properly fit the initial stiffness of the experimental results. It has to be noted that regardless the percentage of the experimental Young's modulus, the variation of the initial stiffness of the entire wall is not quite and it also does not affect too much the nonlinear behaviour of the wall. For instance, whether a value $E^* = 100\%E_0$ had been used instead of $E^* = 65\%E_0$, only a mistake of 14% would have been committed when capturing the initial experimental stiffness of the entire wall. Nevertheless, it must be taken into account that the initial stiffness of the entire walls is due to the contribution of both concrete frames and masonry panel, therefore, the small variation of 14% is due to the fact that only one source of stiffness is being affected. On the other hand, it is worth mentioning that the experimental area showed in Figs. 12–16, turned out from the area enclosed by the experimental curves showed in Fig. 4. Once calibrated

the Young's modulus, masonry's tensile strength was the next parameter to be iterated, as is shown in Fig. 13.

In terms of fitting the nonlinear part of the experimental capacity zone (Fig. 13), it has to be noted the effect of decreasing the tensile strength of masonry, which is related to an earlier cracking of the masonry panel which in turns results in a quicker decreasing of the wall elastic modulus. According to Fig. 13, a value of $t_f = 1.20$ MPa was taken into account for the iteration of the next parameter. Regarding the fracture energy, Fig. 14 shows the numerical curves obtained from iterating this parameter. Like tensile strength, the effect of decreasing this parameter is associated to a quicker cracking process and indeed to a quicker stiffness degradation. These results allowed to conclude that both parameters are linked and govern the nonlinear behaviour of the wall. According to the experimental zone, the value $G_f = 0.10$ N/mm was chosen for showing the best fitting.

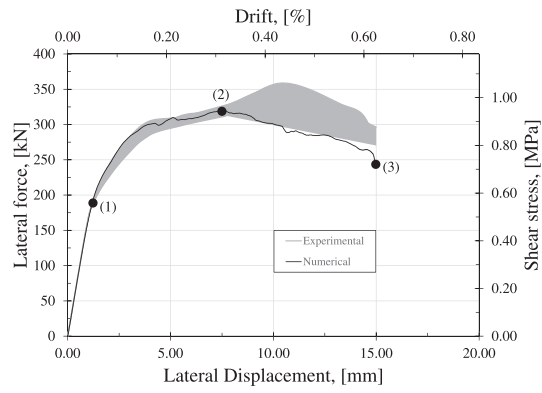
Once calibrated all the material parameters, it turned out important to compare the cracking pattern of both experimental cyclic test and numerical pushover analysis. Fig. 15 shows the cracking pattern for both experimental and numerical tests, according to different performance levels related to: (1) end of linear behaviour, (2) yielding beginning and (3) maximum load capacity.

It has to be noted that there was a good agreement in terms of cracking pattern between half an experimental wall and numerical results by showing bending cracks which occurred first on the confinement column and grew up to the bottom center of the wall. According to the evolution of cracks, in both cases it can be seen how horizontal cracks are propagated in the height of the confinement column whereas the lateral displacement increase. Regarding the beam foundation, it was possible to capture an unexpected bending failure which shows the potential of the proposed model for reproducing all the experimental effects. As it was aforementioned, the foundation could be assumed to be rigid enough in comparison with masonry wall, which implies that all the failure should be concentrated in the wall. However, the lack of bending stiffness of the RC beam foundation led to its unexpected failure which could be properly captured by the proposed model. In addition, it should be noted that the experimental cracking pattern shows additional cracks that can not be captured by a pushover analysis since they are related to the cyclic behaviour of materials. Namely, additional cracks are intended to appear when there are excursions among compressive and tensile states.

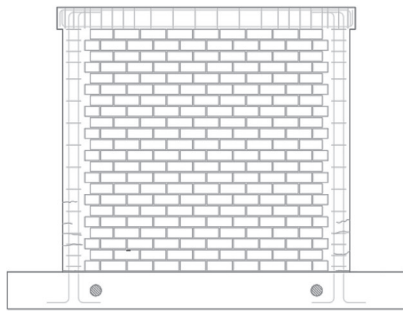
4.2. Walls with vertical load

The calibrated material properties for the case of walls without vertical load, were intended to be used for showing the reliability of the proposed model for fitting the experimental results of another testing setup, which corresponded to consider a vertical load prior the application of lateral loading. This vertical load had a value of 170 kN which tried to represent the weight of 3 stories over a wall located at the first floor. It is worth mentioning that this vertical load was controlled manually by an operator who noted an oscillating variation of the vertical load conforming the lateral displacements were increasing. In fact, this variation became significant from a displacement level of 7.70 mm onwards. That was why the first test with vertical load was stopped for this displacement level (Fig. 4). For the next tests, this vertical load was intended to keep close to the 170 kN as much as possible. However, it was not possible to control which meant a complication for the modelling process to capture the nonlinear behaviour of the walls from the displacement level aforementioned. This oscillating effect of the vertical load caused an increment in the load capacity of the walls which was considered as unreal because it was caused by an uncontrollable boundary condition during their tests.

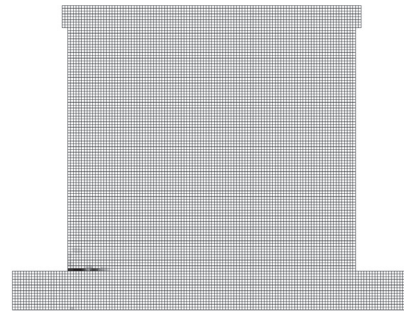
As it was mentioned before, the calibrated material properties from walls without vertical load were used here. However, it was noted that an equivalent Young's modulus of $E^* = 65\%E_0$ did not capture the initial stiffness showed by the experimental results. On contrary, it had to be



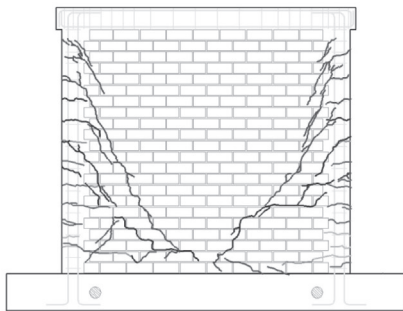
(a) Final numerical curve



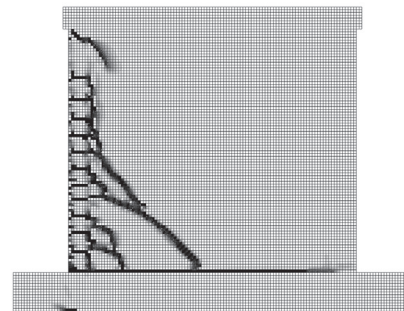
(b) (1) Experimental cyclic test



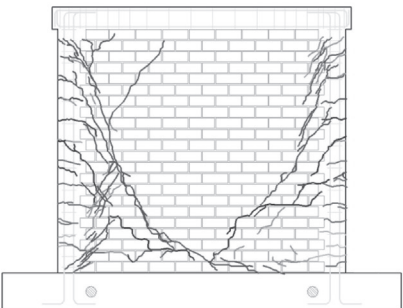
(c) (1) Numerical pushover



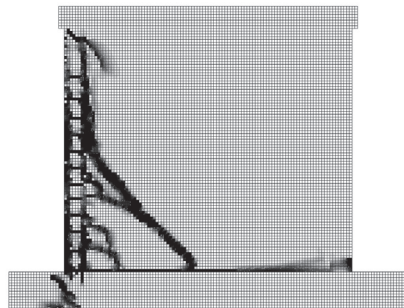
(d) (2) Experimental cyclic test



(e) (2) Numerical pushover



(f) (3) Experimental cyclic test



(g) (3) Numerical pushover

Fig. 17. Experimental and numerical cracking patterns for walls with vertical load ($E^* = 5700$ MPa, $t_f = 1.20$ MPa, $G_f = 0.10$ N/mm).

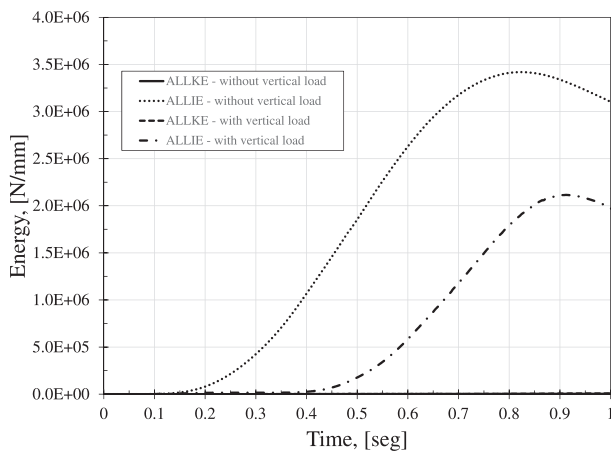


Fig. 18. Comparison of kinetic and internal energies.

used a value of $E^* = 100\%E_0$ to properly fit the initial stiffness of the experimental results (Fig. 16). This variation in percentage is attributed to the fact that each wall, from its construction up to its test, has enough time to develop some micro-cracks which are related to the shrinkage of concrete and mortar, or to the fact that some high stresses can take place during the lifting of the walls. It is known that the presence of cracks is linked to the reduction of the Young's modulus of the materials. However, the presence of vertical load helps to the closing of these cracks which is related to a recovery of this parameter. Anyway, within the showed range 65–100%, it can be highlighted that the variation of Young's modulus does not affect too much the nonlinear response of the wall, as it was noted in Fig. 12 and can also be seen in Fig. 16.

It is important to mention that a proper application of the vertical load should have lead to a behaviour more close to the numerical curve. In fact, a constant vertical load would be more appropriate to represent the load condition of a wall located on the first floor in a real building. To support this idea, it can be seen the results of the experimental tests conducted by Perez et al. [46], where it can clearly seen the tendency of the capacity curves.

Fig. 17 shows the cracking pattern for both experimental and numerical tests, according to different performance levels related to: (1) end of linear behaviour, (2) maximum load capacity and (3) ultimate state. It should be noted there was a good agreement between experimental and numerical cracking pattern until the second analyzed performance level. In the ultimate state, differences are evidenced by the presence of additional cracks, which in fact were produced by the effect of the experimental cyclic loading and the uncontrollable vertical load from second point onwards. Regarding the beam foundation, numerical results showed also a bending failure of the beam foundation, which was not observed experimentally. This effect is entirely attributed to the uncontrollable increment of the applied vertical load which offered a major restriction to the beam foundation against bending.

4.3. Control of dynamic effects

As mentioned before, the quasi-static problem was intended to be solved by means of a purely dynamic explicit solver. For this purpose, the loads were applied by defining smooth step amplitudes, which has the advantage of having zero velocity in the application of the loading at the beginning and ending of the load step. In addition, these smooth steps allow gradually increasing the application of the loading, which helps to minimize kinematic effects. Subsequently, in order to be sure that the numerical results resulted mainly from quasi-static effects, i.e. that kinematic effects were not dominant, the kinetic and internal energy of the whole model (ALLKE and ALLIE, respectively) were compared over the entire time step (Fig. 18). Note that the kinetic energy curves are very close to the axle time. In fact, they were less than 1% of

the internal energy over the largest part of the time step, which allowed being sure that the numerical results were not influenced by kinetic effects.

5. Conclusion

A 3D finite element model based on the macro-modelling technique was presented to simulate the nonlinear behaviour of confined masonry walls subjected to in-plane lateral loading. For this purpose, all the solid elements were modelled as single parts, which means that no contact surfaces between the different materials were physically modelled. In addition, due to the assumptions made by Concrete Damage Plasticity (CDP) of treating quasi-brittle materials as isotropic, it was not possible to use the material properties directly obtained from small sample tests. On the contrary, these materials properties needed to be calibrated. After many iterations, varying the material properties of the concrete and masonry, it was concluded that the main parameters that controlled the nonlinear behaviour of the walls were the Young's modulus, tensile strength and fracture energy of the masonry. Therefore, in a parametric study, these parameters were iteratively varied until reaching a good fit of the experimental results.

1. Recalling that Young's modulus, E_0 , of masonry was obtained experimentally by means of the well-known compressive tests of brick prisms, it could be seen that values of $65\%E_0$ and $100\%E_0$ properly fit the initial stiffness of walls without and with vertical load, respectively. In fact, Young's modulus is related to the presence of cracks prior to testing, but anyway the impact of fitting the initial stiffness with a more or a little less precision does not affect too much the nonlinear response of the confined masonry walls.
2. Regarding the tensile strength and fracture energy of the masonry, it is worth mentioning that both parameters controlled the cracking pattern and the nonlinear behaviour of the confined masonry walls. Therefore, they were iterated together so as to obtain a reduced value of $t_f = 1.20$ MPa, instead of the $t_f = 1.40$ MPa obtained from the well-known diagonal compressive test of square masonry samples, and a fracture energy of $G_f = 0.10$ N/mm, which allowed properly fitting both the cracking pattern and the nonlinear part of the capacity curves.
3. Finally, the proposed model achieved good precision in capturing the nonlinear response of confined masonry walls as well as their cracking pattern. Therefore, taking into account the efficiency and the simplicity of the application of the model herein proposed, it can be concluded that it can be used to help laboratory tests and designing codes in case it is important to predict the cracking patterns, maximum load capacity, and the ultimate displacements of confined masonry walls.

Declaration of Competing Interest

The authors declared that there is no conflict of interest.

Acknowledgment

The authors wish to acknowledge the economic support provided by CONCYTEC within the framework of the N° 232-2015-FONDECYT Agreement.

References

- [1] INEI. Censos nacionales 2014: población y vivienda. Instituto nacional de estadística e informática; 2014.
- [2] E070. Reglamento nacional de edificaciones: Albañilería, Ministerio de Vivienda, Construcción y Saneamiento - SENCICO; 2006.
- [3] Lara J, León J. <https://elcomercio.pe/lima/sucesos/viviendas-construidas-ladrillos-pandereta-riesgo-sismos-lima-noticia-464070?foto=1>; 2017.
- [4] El-Diasy M, Okail H, Kamal O, Said M. Structural performance of confined

- masonry walls retrofitted using ferrocement and GFRP under in-plane cyclic loading; 2015:54–69.
- [5] Wijaya W, Kusumastuti D, Suarjana M, Pribadi K, et al. Experimental study on wall-frame connection of confined masonry wall. *Procedia Eng* 2011;14:2094–102.
- [6] Kassem N, Atta A, Etman E. Structural behavior of strengthening masonry in-filled frames subjected to lateral load using bonded and un-bonded CFRP. *KSCSE J Civil Eng* 2016;21(3):818–28.
- [7] Breveglieri M, Camata G, Spacone E. Strengthened infilled RC frames: Continuum and macro modeling in nonlinear finite element analysis. *Compos Part B: Eng* 2018.
- [8] Lovon H, Tarque N, Silva V, Yepes-Estrada C. Development of Fragility Curves for Confined Masonry Buildings in Lima, Peru. *Earthq Spectra* 2018;34(3):1339–61.
- [9] D'Amato M, Laterza M, Diaz Fuentes D. Simplified seismic analyses of ancient churches in matera's landscape. *Int J Archit Heritage* 2018:1–20.
- [10] Singhal V, Rai DC. In-plane and out-of-plane behavior of confined masonry walls for various toothing and openings details and prediction of their strength and stiffness. *Earthq Eng Struct Dyn* 2016;45(15):2551–69.
- [11] Al-Chaar G. Evaluating strength and stiffness of unreinforced masonry infill structures. Tech. Rep., Engineer Research and Development Center, US Army Corps of Engineers, Construction Engineering Research Laboratory TR-02-1; 2002.
- [12] Lourenço PJBB. Computational strategies for masonry structures; 1997.
- [13] Tarque N, Camata G, Varum H, Spacone E, Blondet M. Numerical simulation of an adobe wall under in-plane loading. *Earthq Struct* 2014;6(6):627–46.
- [14] Okail H, Abdelrahman A, Abdelkhalik A, Metwaly M. Experimental and analytical investigation of the lateral load response of confined masonry walls. *J Housing Build Nat Res Center* 2016;12:33–46.
- [15] Annechiarico M, Portioli F, Landolfo R. Micro and macro finite element modeling of brick masonry panels subject to lateral loadings. In: Proc., COST C26 Action Final Conf; 2010, p. 315–20.
- [16] Gatta C, Addessi D, Vestroni F. Static and dynamic nonlinear response of masonry walls. *Int J Solids Struct* 2018;155:291–303.
- [17] D'Altri AM, de Miranda S, Castellazzi G, Sarhosis V. A 3d detailed micro-model for the in-plane and out-of-plane numerical analysis of masonry panels. *Comput Struct* 2018;206:18–30.
- [18] Nasiri E, Liu Y. Development of a detailed 3D FE model for analysis of the in-plane behavior of masonry infilled concrete frames. *Eng Struct* 2017;143:603–16.
- [19] Aref AJ, Dolatshahi KM. A three-dimensional cyclic meso-scale numerical procedure for simulation of unreinforced masonry structures. *Comput Struct* 2013;120:9–23.
- [20] Bolhassani M, Hamid AA, Lau AC, Moon F. Simplified micro modeling of partially grouted masonry assemblages. *Constr Build Mater* 2015;83:159–73.
- [21] Manchego J, Pari S. Análisis experimental de muros de albañilería confinada en viviendas de baja altura en Lima, Perú Master's thesis Pontificia Universidad Católica del Perú; 2016.
- [22] Goto Y, Kumar GP, Kawanishi N. Nonlinear finite-element analysis for hysteretic behavior of thin-walled circular steel columns with in-filled concrete. *J Struct Eng* 2010;136(11):1413–22.
- [23] Lee J, Fenves G. Plastic-damage model for cyclic loading of concrete structures. *J Eng Mech* 1998;124(8):892–900.
- [24] Jankowiak T, Lodygowski T. Identification of parameters of concrete damage plasticity constitutive model. *Found Civil Environ Eng* 2005;6(1):53–69.
- [25] Abaqus. Ver. 6.14 Documentation, Dassault Systems Simulia Corporation; 2014.
- [26] Michałs, Andrzej W. Calibration of the CDP model parameters in ABAQUS; 2015.
- [27] Anderson TL. Fracture mechanics: fundamental and applications. CRC Press; 2005.
- [28] CEB-FIP. Model code 2010, London: Thomas Telford; 2010.
- [29] Krätzig WB, Pölling R. An elasto-plastic damage model for reinforced concrete with minimum number of material parameters. *Comput Struct* 2004;82(15–16):1201–15.
- [30] Alfarah B, López-Almansa F, Oller S. New methodology for calculating damage variables evolution in Plastic Damage Model for RC structures. *Eng Struct* 2017;132:70–86.
- [31] Hordijk DA. Tensile and tensile fatigue behaviour of concrete; Experiments, modelling and analyses. *Heron* 1992;37(1).
- [32] Oller S. A continuous damage model for frictional materials Ph.D. thesis, Doctoral Dissertation Technical University of Catalonia; 1988.
- [33] Kaushik HB, Rai DC, Jain SK. Stress-strain characteristics of clay brick masonry under uniaxial compression. *J Mater Civ Eng* 2007;19(9):728–39.
- [34] Agnihotri P, Singhal V, Rai DC. Effect of in-plane damage on out-of-plane strength of unreinforced masonry walls. *Eng Struct* 2013;57:1–11.
- [35] Hillerborg A, Modéer M, Petersson P-E. Analysis of crack formation and crack growth in concrete by means of fracture mechanics and finite elements. *Cem Concr Res* 1976;6(6):773–81.
- [36] Dehestani M, Mousavi S. Modified steel bar model incorporating bond-slip effects for embedded element method. *Constr Build Mater* 2015;81:284–90.
- [37] Monti G, Filippou FC, Spacone E. Finite element for anchored bars under cyclic load reversals. *J Struct Eng* 1997;123(5):614–23.
- [38] Sezen H, Setzler EJ. Reinforcement slip in reinforced concrete columns. *ACI Struct J* 2008;105(3):280.
- [39] Braga F, Gigliotti R, Laterza M, D'Amato M, Kunnath S. Modified steel bar model incorporating bond-slip for seismic assessment of concrete structures. *J Struct Eng* 2012;138(11):1342–50.
- [40] D'Amato M, Braga F, Gigliotti R, Kunnath S, Laterza M. Validation of a modified steel bar model incorporating bond-slip for seismic assessment of concrete structures. *J Struct Eng* 2012;138(11):1351–60.
- [41] Park YJ, Reinhorn AM, Kunnath SK. IDARC: Inelastic damage analysis of reinforced concrete frame-shear-wall structures; 1987.
- [42] Abdullah R, Paton-Cole V, Easterling W, ASCE F. Quasi-static analysis of composite slab, Malaysian. *J Civil Eng* 2007;19(2):1–13.
- [43] Karapitta L, Mouzakis H, Carydis P. Explicit finite-element analysis for the in-plane cyclic behavior of unreinforced masonry structures. *Earthq Eng Struct Dyn* 2011;40(2):175–93.
- [44] Tarque N, Camata G, Spacone E, Varum H, Blondet M. Nonlinear dynamic analysis of a full-scale unreinforced adobe model. *Earthq Spectra* 2014;30(4):1643–61.
- [45] Medeiros P, Vasconcelos G, Lourenço PB, Gouveia J. Numerical modelling of non-confined and confined masonry walls. *Constr Build Mater* 2013;41:968–76.
- [46] Pérez Gavilán JJ, Flores L, Alcocer S. Efecto de la esbeltez en la resistencia de muros de mampostería confinada. *Ingeniería Sísmica* 2013(89):55–76.